NASA CR- 73390
AVAILABLE TO THE PUBLIC

THE DYNAMIC BEHAVIOR OF ROTOR ENTRY VEHICLE CONFIGURATIONS I. EQUATIONS OF MOTION

By A. Z. Lemnios and N. Giansante

Kaman Report No. R-767-1

November 1968

Distribution of this report is provided in the interest of information exchange. Responsibility for the contents resides in the author or organization that prepared it.

Prepared Under Contract No. NAS 2-3917 By

KAMAN AIRCRAFT
DIVISION OF KAMAN CORPORATION
Bloomfield, Connecticut

For

NATIONAL AERONAUTICS AND SPACE ADMINISTRATION

FACILITY FORM 602

N70-14187 (ACCESSION NUMBER)
38 (PAGES)
CR-73390 (NASA CR OR TMX OR AD NUMBER)
1 (THRU)
(CODE)
01 (CATEGORY)

PRECEDING PAGE BLANK-NOT FILMED

SUMMARY

A theoretical analysis has been conducted to study the dynamic behavior and aerodynamic characteristics of a rotor in autorotative flight operating in proximity of a reentry capsule. A mathematical model representing the rotor entry vehicle was established, the necessary equations formulated and computer programs were generated for solution of this system.

The equations of motion describing the articulated rotor blades retained all nonlinear inertial terms and incorporated nonlinear aerodynamics to account for stall, compressibility and reversed flow effects. Provisions were also included to consider the effects on the rotor of the detached bow shock wave generated by the capsule.

The equations of motion for vehicle dynamic stability were written to include coupling effects between capsule body motion and rotor forces and moments. Numerical time histories of the coupled rotor entry vehicle system are calculated at time increments specified by the user.

PRECEDING PAGE BLANK NOT FILMED.

TABLE OF CONTENTS

LIST OF SYMBOLS

a	Rotor blade airfoil lift curve slope
a_∞	Free stream speed of sound
A	Hyperbolic bow wave semi-transverse axis
A_C	Longitudinal offset between rotor shaft and vehicle center of gravity
A_D	Longitudinal offset between rotor shaft and vehicle balance center
b	Number of rotor blades
B_C	Vertical offset between heat shield center and vehicle center of gravity
B_D	Vertical offset between heat shield center and body balance center
B_{eq}	Vertical offset between rotor hub and center of equivalent capsule sphere
B_M	Vertical offset between heat shield center and data reference center
B_R	Vertical offset between heat shield center and rotor hub
c	Local blade chord
c_o	Blade chord reference
C_D, C_L, C_m	Blade airfoil drag, lift, and pitching moment coefficients
$C_{D_{RC}}$, $C_{L_{RC}}$, $C_{m_{RC}}$	Capsule body drag, lift, and pitching moment coefficients. Body aerodynamic data are considered at data reference center
C_β, C_ζ, C_θ	Damper rates for blade flapping, lagging, and feathering degrees of freedom
D, L	Local blade section drag and lift forces
D_B, L_B	Capsule body drag and lift forces
e_1	Rotor lag hinge offset ($\bar{e}_1 = \frac{e_1}{R}$)

e_2	Rotor flapping hinge offset ($\bar{e}_2 = \frac{e_2}{R}$)
$F_{x_B}, F_{y_B}, F_{z_B}, M_{x_B}, M_{y_B}$	Capsule body forces and moments
$F_{x_R}, F_{y_R}, F_{z_R}, M_{x_R}, M_{y_R}$	Rotor hub forces and moments
g	Acceleration due to gravity
H, T, Y	Rotor horizontal, thrust, and side forces
$I_1, \ldots I_5, S_1, \ldots, S_3, M$	Rotor blade inertia characteristics defined in Equation (A1)
I_R	Rotor polar moment of inertia
$I_{xx}, I_{yy}, I_{zz}, I_{xz}$	Capsule body moments of inertia and cross product of inertia about body axes
K_β, K_ζ, K_θ	Spring rates for blade flapping, lagging, and feathering degrees of freedom
$K_{\theta_{IN}}$	Spring rate for blade feathering input control system
$K_{\theta\beta}$, $K_{\theta\zeta}$	Mechanical coupling between blade feathering/flapping and feathering/ lagging degrees of freedom
M_∞	Free stream Mach number
p, q	Roll and pitch rates in rotor axis system
p_B, q_B, r_B	Roll, pitch, and yaw rates in body axis system
Q	Rotor torque due to airloads
Q_β, Q_ζ, Q_θ	Generalized forces in blade flapping, lagging, and feathering degrees of freedom
r	Local blade section radius (x = r/R)

R	Total blade radius
R_c	Radius of equivalent circular reference area
u_B, v_B, w_B	Vehicle linear velocities in body axis system
U_P, U_T	Perpendicular and tangential components of local blade section relative air velocity
V_∞	Vehicle total free stream velocity
x_B, y_B, z_B	Body coordinate axis system
x_E, y_E, z_E	Flat earth coordinate axis system
x_R, y_R, z_R	Rotor coordinate axis system
α	Local blade section angle of attack
α_R	Rotor shaft and vehicle body angle of attack
β, ζ, θ	Blade flapping, lagging, and feathering degrees of freedom
$\beta_o, \zeta_o, \theta_o$	Blade flapping, lagging, and feathering index angles for zero spring loads
γ	Blade Lock number, $\rho acR^4/I_1$
Δ	Stand-off distance between equivalent capsule sphere and bow wave
η	Angle between relative wind and the x body axis
θ_c, θ_{1c}, θ_{1s}	Collective and cyclic components of blade feathering input where the blade feathering motion with respect to the plane normal to the rotor shaft is given by $\theta = \theta_o - \theta_{1c}\cos\psi - \theta_{1s}\sin\psi$
θ_{IN}	Total blade feathering input
θ_x	Blade built-in twist distribution
Θ_E, Φ_E, Ψ_E	Vehicle orientation angles referenced to flat earth axis system
λ	Rotor inflow ratio
μ	Rotor advance ratio

ξ	Blade section center of gravity chord distance referenced to blade feathering axis
ξ_a	Blade section aerodynamic center chord distance referenced to blade feathering axis
ρ	Free stream air density
ρ_*	Air density at point of intersection between bow shock wave and forward rotor blade
ρ_ψ	Air density variation behind shock wave around azimuth
σ	Rotor solidity
ϕ	Local blade section inflow angle
ψ	Rotor azimuth position
Ω	Rotor angular speed

LIST OF FIGURES

INTRODUCTION

Background

Modern aerospace programs have imposed a need for improved performance and control capabilities of recovery systems. More accurate flight path control during the reentry phase, improved maneuverability during descent, lower touchdown velocities, and control of the landing mode are sought.

A concept that has demonstrated capabilities for these advanced recovery functions is the unpowered rotary wing decelerator - a multibladed, helicopter-type rotor which provides aerodynamic retardation and control in autorotative descent. Rotary wing decelerators can be incorporated in a single-stage system for low or high speed deployment, retardation and stabilization, drag force modulation, flight path maneuverability, and landing with effectively zero vertical and horizontal speeds.

State of the Art

The potential of rotary wing decelerators has been demonstrated successfully at subsonic speeds in a USAF-sponsored flight test program during which decelerators were dropped at speeds up to 550 knots (Reference 1). A wind tunnel test phase of this program also demonstrated that rotors can be deployed and operated in axial descent at speeds up to Mach numbers of 3.0 (Reference 2). Recent wind tunnel investigations by NASA (Reference 3) have successfully expanded the operating regimes of rotary wing decelerators to glide flight at Mach numbers up to 3.5. A detailed summary of the state of the art is presented in Reference 4.

The various flight tests and wind tunnel tests mentioned above will be enhanced with the complementary use of a rotor analysis which will predict blade airloads, blade dynamics, rotor performance, and vehicle stability for a rotor entry vehicle system throughout its flight spectrum. Available helicopter rotor analyses (e.g., Reference 5) have been concerned with powered rotors in subsonic flight. As such, they are not directly usable for studying autorotative rotors in supersonic flight; consequently, they must be modified and extended to investigate autorotating rotors at these extreme operating conditions.

Program Goals

The analysis described herein was undertaken to provide NASA with the analytical tools to evaluate rotor entry vehicle systems thereby permitting trade-off studies between rotary wing decelerators and present day decelerators. Furthermore, results of the program will be useful in identifying areas of research in rotary wing decelerator technology that require further investigation analytically and experimentally.

Problem Definition

As mentioned previously, the present state of the art of rotor technology must be advanced to examine rotor and vehicle dynamic behavior at transonic and supersonic speeds. Theories already developed for powered rotors in the subsonic regime were used as stepping stones in developing the advanced theories and computer programs for predicting the performance, dynamics, and stability of autorotating rotors. The key step in the development of the new theories and programs is the formulation of a valid blade airloads and rotor performance analysis. Only by having reasonable estimates of rotor performance and airloads can any confidence be placed in analytical predictions of rotor and vehicle system dynamics and stability.

Consequently, the analyses in the present program are subdivided to evaluate rotor stability, rotor airloads and performance, and vehicle dynamic stability. Descriptions of these analyses and their equations of motion are presented in the ensuing sections.

ROTOR STABILITY, AIRLOADS, AND PERFORMANCE

Method of Analysis

A systematic method of analysis was developed in Reference 5 for the derivation of the general nonlinear equations of motion of a rotor blade with five degrees of blade freedom under both steady and maneuvering flight conditions. This method incorporates a position matrix which transforms point mass coordinates from a rotating axis system to a fixed axis system by finite rotations for each degree of freedom. These position matrices are orthogonal. Hinge offsets are obtained by matrix translations.

In the matrix method of analysis the transformed point mass coordinates are differentiated to obtain velocities and accelerations resulting from each degree of freedom. The velocities and accelerations are combined to yield the inertial and centrifugal terms in the blade equations of motion. The blade forces and moments associated with the control springs and retention springs and dampers are added to these acceleration terms thereby resulting in the complete, nonlinear, free equations of motion. The forced equations of motion are obtained by applying generalized forces which incorporate experimental aerodynamic coefficients.

The aerodynamic characteristics are a function of angle of attack, Mach number, and radial station. The unsteady aerodynamic forces and moments are included in the forcing function as an approximation.

Equations of Motion

Figure 1 shows a deflected, twisted rotor blade assumed to have flapping, feathering, and lagging degrees of freedom. The coordinate transformation matrices are obtained by considering an axis system initially on the blade feathering axis. The axes are then rotated and translated sequentially until they are coincident with the rotor shaft and are translating through space. The complete expression for the displacement matrix is obtained by combining the coordinate transformations. Velocity and acceleration matrices are defined by differentiating the displacement matrix. The final equations of motion evolving from these matrices are derived in detail in Reference 5 and are presented below.

Flapping.-

$$\left\{e_1\left[S_1 \$_\beta - (S_2 \mathbb{C}_\theta + S_3 \$_\theta)\mathbb{C}_\beta\right]\mathbb{C}_\zeta\right\}\Omega^2$$
$$+\left\{(e_2-e_1)\left[S_1\$_\beta-(S_2\mathbb{C}_\theta+S_3\$_\theta)\mathbb{C}_\beta\right]+\left[I_1-I_5\$_\theta^2\right]\$_\beta\mathbb{C}_\beta\right.$$
$$\left.+\left[I_2\mathbb{C}_\theta+I_3\$_\theta\right](\$_\beta^2-\mathbb{C}_\beta^2)\right\}(\Omega+\dot\zeta)^2$$
$$+2\left\{\left[I_2\mathbb{C}_\theta+I_3\$_\theta\right]\$_\beta-I_5\$_\theta^2\mathbb{C}_\beta\right\}(\Omega+\dot\zeta)\dot\theta$$
$$+2\left\{I_5\$_\theta\mathbb{C}_\theta\right\}\dot\beta\dot\theta+\left\{I_2\mathbb{C}_\theta+I_3\$_\theta\right\}\dot\theta^2$$
$$+\left\{\left[I_2\$_\theta-I_3\mathbb{C}_\theta\right]\$_\beta+I_5\$_\theta\mathbb{C}_\theta\mathbb{C}_\beta\right\}\ddot\zeta$$
$$+\left\{I_1+I_5\$_\theta^2\right\}\ddot\beta+\left\{I_2\$_\theta-I_3\mathbb{C}_\theta\right\}\ddot\theta$$
$$+\left\{I_1+e_2S_1\right\}\left\{2p\Omega\mathbb{C}_\psi+2q\Omega\$_\psi\right\}\mathbb{C}_\beta^2+I_3\left\{2q\Omega\mathbb{C}_\psi-2p\Omega\$_\psi\right\}$$
$$+K_\beta(\beta-\beta_0)-K_{\theta_{IN}}K_{\theta\beta}(\theta-\theta_{IN})+C_\beta\dot\beta=Q_\beta \qquad (1)$$

Feathering.-

$$\left\{e_1\left[(S_2\mathbb{C}_\theta+S_3\$_\theta)\$_\zeta-(S_3\mathbb{C}_\theta-S_2\$_\theta)\mathbb{C}_\zeta\$_\beta\right]\right\}\Omega^2$$
$$+\left\{-(e_2-e_1)(S_3\mathbb{C}_\theta-S_2\$_\theta)\$_\beta-(I_3\mathbb{C}_\theta-I_2\$_\theta)\$_\beta\mathbb{C}_\beta\right.$$
$$\left.+I_5\$_\theta\mathbb{C}_\theta\mathbb{C}_\beta^2\right\}(\Omega+\dot\zeta)^2+2\left\{I_5\$_\theta^2\mathbb{C}_\beta-(I_2\mathbb{C}_\theta+I_3\$_\theta)\$_\beta\right\}(\Omega+\dot\zeta)\dot\beta$$
$$-2\left\{I_5\$_\theta\mathbb{C}_\theta\right\}\dot\beta^2-\left\{I_3\mathbb{C}_\theta-I_2\$_\theta\right\}\ddot\beta+\left\{I_4\right\}\ddot\theta+\left\{(e_2-e_1)\left[S_3\$_\theta+S_2\mathbb{C}_\theta\right]\right.$$
$$\left.+\left[I_2\mathbb{C}_\theta+I_3\$_\theta\right]\mathbb{C}_\beta+I_4\$_\beta\right\}\ddot\zeta+\left\{I_3+e_2S_3\right\}\left\{2q\Omega\$_\psi+2p\Omega\mathbb{C}_\psi\right\}$$
$$+\left\{I_5\right\}\left\{2q\Omega\mathbb{C}_\psi-2p\Omega\$_\psi\right\}+K_\theta(\theta-\theta_0)+K_{\theta_{IN}}(\theta-\theta_{IN})+C_\theta\dot\theta=Q_\theta \qquad (2)$$

Lagging.-

$$\{e_1(e_2-e_1)M\$_\zeta+e_1[S_1\mathbb{C}_\beta\$_\zeta+(S_2\mathbb{C}_\theta+S_3\$_\theta)\$_\beta\$_\zeta-(S_3\mathbb{C}_\theta-S_2\$_\theta)\mathbb{C}_\zeta]\}\Omega^2$$
$$+2\{(e_2-e_1)[-S_1\$_\beta+(S_2\mathbb{C}_\theta+S_3\$_\theta)\mathbb{C}_\beta]-I_1\$_\beta\mathbb{C}_\beta-[I_2\mathbb{C}_\theta+I_3\$_\theta](\mathbb{C}_\beta^2-\$_\beta^2)$$
$$+I_5\$_\theta^2\$_\beta\mathbb{C}_\beta\}(\Omega+\dot\zeta)\dot\beta+2\{(e_2-e_1)(S_3\mathbb{C}_\theta-S_2\$_\theta)\$_\beta+[I_3\mathbb{C}_\theta-I_2\$_\theta]\$_\beta\mathbb{C}_\beta$$
$$-I_5\$_\theta\mathbb{C}_\theta\mathbb{C}_\beta^2\}(\Omega+\dot\zeta)\dot\theta+\{(I_2\$_\theta-I_3\mathbb{C}_\theta)\mathbb{C}_\beta-I_5\$_\theta\mathbb{C}_\theta\$_\beta\}\dot\beta^2+2\{I_5\mathbb{C}_\theta^2\mathbb{C}_\beta\}\dot\beta\dot\theta$$
$$+\{(e_2-e_1)(S_3\mathbb{C}_\theta-S_2\$_\theta)+(I_3\mathbb{C}_\theta-I_2\$_\theta)\mathbb{C}_\beta\}\dot\theta^2+\{(I_2\$_\theta-I_3\mathbb{C}_\theta)\$_\beta$$
$$+I_5\$_\theta\mathbb{C}_\theta\mathbb{C}_\beta\}\ddot\beta+\{(e_2-e_1)(S_3\$_\theta+S_2\mathbb{C}_\theta)+(I_2\mathbb{C}_\theta+I_3\$_\theta)\mathbb{C}_\beta+I_4\$_\beta\}\ddot\theta$$
$$+\{(e_2-e_1)^2M+2(e_2-e_1)[S_1\mathbb{C}_\beta+(S_2\mathbb{C}_\theta+S_3\$_\theta)\$_\beta]+I_1\mathbb{C}_\beta^2$$
$$+(I_2\mathbb{C}_\theta+I_3\$_\theta)\$_\beta\mathbb{C}_\beta+I_5(\mathbb{C}_\theta^2+\$_\theta^2\$_\beta^2)\}\ddot\zeta+K_\zeta(\zeta-\zeta_0)+C_\zeta\dot\zeta \qquad (3)$$
$$-K_{\theta_{IN}}K_{\theta\zeta}(\theta-\theta_{IN})=Q_\zeta$$

The inertias and generalized forces in Equations (1) - (3) are summarized in Appendix A. For sake of convenience, the following symbolism was also used in these equations and will be retained throughout the vehicle stability analysis.

$$\$_U=\text{sine}_U \qquad \mathbb{C}_U=\text{cosine}_U$$

The feathering input is given by:

$$\theta_{IN}=\theta_C-\vartheta_{1S}\$_\Psi-\theta_{1C}\mathbb{C}_\Psi+K_{\theta\beta}\beta+K_{\theta\zeta}\zeta$$

Numerical Solution

Numerical methods of solution for the previous differential equations of motion are derived in Reference 5. The techniques described therein are used to generate response matrices, evaluate transient responses to an initial disturbance, and iterate until periodic solutions are achieved which include nonlinear inertial and aerodynamic effects.

The converged periodic solutions yield azimuthal variations of blade kinematics and radial and azimuthal variations of blade airloads. These distributions are used in the following expressions to calculate rotor torque, thrust, horizontal and side force.

$$Q = \frac{b}{2\pi} \int_0^{2\pi} \int_{e_1}^{R} (L\$_\phi + D\mathbb{C}_\phi) r\,dr\,d\psi \tag{4}$$

$$T = \frac{b}{2\pi} \int_0^{2\pi} \int_{e_1}^{R} (L\mathbb{C}_\phi + D\$_\phi)\mathbb{C}_\beta\,dr\,d\psi \tag{5}$$

$$H = \frac{b}{2\pi} \int_0^{2\pi} \int_{e_1}^{R} \left[(L\$_\phi + D\mathbb{C}_\phi)\$_\psi - (L\mathbb{C}_\phi + D\$_\phi)\$_\beta \mathbb{C}_\psi\right] dr\,d\psi \tag{6}$$

$$Y = \frac{b}{2\pi} \int_0^{2\pi} \int_{e_1}^{R} -\left[(D\mathbb{C}_\phi - L\$_\phi)\,\mathbb{C}_\psi + (L\mathbb{C}_\phi + D\$_\phi)\$_\beta \$_\psi\right] dr\,d\psi \tag{7}$$

Because the analysis is written to evaluate an unpowered rotor, the equilibrium torque, as defined by Equation (4), must be zero. Consequently, at a particular rotor operating condition, the blade pitch angle must be determined to effect zero torque. If the torque does not vanish at a preselected operating condition, a torque iteration procedure automatically changes blade pitch setting until the torque constraint is satisfied.

Initially, the method employs a derivative to estimate the second trial pitch angle. The value of the derivative is obtained by using linearized rotor theory (Reference 6) and is given by

$$\frac{dQ}{d\theta} = -\frac{\pi}{6} \rho a \sigma \lambda \Omega^2 R^5 \tag{8}$$

Thus, the second trial value of pitch angle is

$$\theta_2 = \theta_1 - \frac{Q_1}{\left(\frac{dQ}{d\theta}\right)} \tag{9}$$

Numerical values for the derivative are obtained from the calculations using the first trial value of blade pitch setting.

The third trial value of blade pitch angle is estimated by using a first-order difference equation which is based on the first two calculations.

$$\theta_3 = \theta_2 - \frac{Q_2}{\left(\frac{Q_2 - Q_1}{\theta_2 - \theta_1}\right)} \tag{10}$$

The fourth and subsequent trial values of blade angle are determined from the following second order curve.

$$Q = a_2\theta^2 + a_1\theta + a_0 \tag{11}$$

A collocation procedure is used to evaluate the a - coefficients in Equation (11). For equilibrium conditions, the torque must vanish and new values of θ are obtained from the above quadratic.

As the torque iteration continues, the three most recent values of torque and respective blade angles are retained to evaluate the next trial value for blade pitch angle. A tolerance on torque supplied to the computer program as input is employed to determine autorotative equilibrium. Retardation of the rotor due to bearing friction was omitted from the computations.

Supersonic Inflow Through The Rotor

A rotary wing that is used as a retardation system on a reentry vehicle will operate through a shock wave generated by the capsule during a portion of its trajectory. At transonic and supersonic speeds, the rotor blades will be operating in and out of the shock wave envelope generated by the capsule.

For simplicity, the capsule is assumed to be a sphere which produces an axially symmetric bow wave as illustrated in Figure 2. In order to define which portion of the rotor is operating ahead of and which part is operating aft of the shock wave, the line of intersection between the detached bow shock wave generated by the capsule and the rotor cone must be determined.

The shape of the detached bow wave may be expressed analytically using the approximate method of Moeckel as reported in Reference 7. Moeckel has indicated that a spherical body

generates a shock wave which can be satisfactorily approximated by a hyperboloid of revolution with its axis parallel to the remote relative wind. The intersection of the hyperboloid and the rotor surfaces defines the boundary between disturbed and undisturbed flow; the blade flapping response is considered in the determination of this boundary. Thus, the line of intersection becomes a function of blade radial station and azimuth location. Equations which define the boundary line are presented in Appendix B.

The disturbed flow conditions behind the shock wave are evaluated by the oblique shock equations of Reference 8. The shock wave angle at rotor azimuth position of 180 degrees is used as a control point to determine shock strength. New velocities and densities are evaluated behind the shock using this control point and the advance ratio and inflow ratio distribution are reevaluated. Because of expansion behind the shock wave, the air density was also assumed to vary with azimuth and rotor angle of attack according to the following relation

$$\rho_\psi = \left\{ \rho_\pi V_\pi^2 (1 - .5 \$_{a_R}) + .5 \left[.2 \rho_\infty V_\infty^2 (1 + 3 \mathbb{C}_{a_R}) - \rho_\pi V_\pi^2 (1 - .5 \$_{a_R}) \right] \mathbb{C}_{a_R}^2 (1 + C_\psi) \right\} / U^2 \qquad (12)$$

The effects of flow turning behind the bow wave and the effects of mutual shock interference between adjacent blades were neglected.

VEHICLE DYNAMIC STABILITY

Equations of Motion

The six basic equations of motion necessary to describe the dynamic behavior of the rotor entry vehicle shown in Figure 3 are formulated in detail in Reference 9. These basic equations are modified to include rotor forces and moments. The modified equations are written for a right-hand coordinate system with the origin at the vehicle center of gravity. The coordinate systems for the vehicle and rotor are shown in Figure 6. All rotor hub forces and moments are resolved from the rotor axes to the body axes; the rotor axes are defined so that the relative free stream velocity lies in the X_R-Z_R plane. Furthermore, the vehicle was assumed to be symmetrical with respect to the X_B-Z_B plane thereby eliminating the capsule body cross-products of inertia, I_{xy} and I_{yz}.

The orientation angles between moving earth axes and body axes are indicated in Figure 7. The fixed earth axes is also portrayed in the figure, and is used as a reference for the gravity force.

A seventh equilibrium equation is required to complete the vehicle stability analysis. This latter equation defines the rotor angular acceleration in terms of the applied aerodynamic torque and the vehicle yaw acceleration. The complete system of seven equations is summarized below.

$$M_B(\dot{u}_B - v_B r_B + w_B q_B) = F_{x_B} + M_B g \$_{\theta_E} + F_{x_R} \tag{13}$$

$$M_B(\dot{v}_B - w_B p_B + u_B r_B) = F_{y_B} - M_B g \mathbb{C}_{\theta_E} \$_{\Phi_E} + F_{y_R} \tag{14}$$

$$M_B(\dot{w}_B - u_B q_B + v_B p_B) = F_{z_B} - M_B g \mathbb{C}_{\theta_E} \mathbb{C}_{\Phi_E} + F_{z_R} \tag{15}$$

$$\dot{p}_B I_{xx} - \dot{r}_B I_{xz} + (I_{zz} - I_{yy}) q_B r_B - p_B q_B I_{xz} = M_{x_B} + M_{x_R} - (B_R - B_C) F_{y_R} - (B_M - B_C) F_{y_B} \tag{16}$$

$$\dot{q}_B I_{yy} + r_B p_B (I_{xx} - I_{zz}) + (p_B^2 - r_B^2) I_{xz} = M_{y_B} + M_{y_R} + (B_R - B_C) F_{x_R} + A_C (F_{z_R} + F_{z_B}) + (B_M - B_C) F_{x_B} \tag{17}$$

$$\dot{r}_B I_{zz} - \dot{p}_B I_{xz} + (I_{yy} - I_{xx}) p_B q_B + I_{xz} q_B r_B = - A_c (F_{y_R} + F_{y_B}) \qquad (18)$$

$$\dot{r}_B - \dot{\Omega} = \frac{Q}{I_R} \qquad (19)$$

Methods of Solution

The preceding differential equations are solved for accelerations in Appendix C. The resulting accelerations are used in a self-starting, multistep, predictor-corrector integration procedure (Reference 10) to evaluate numerically vehicle velocities and displacements relative to the body axes. In turn, these body axis kinematic components are integrated to yield translational and rotational displacements with respect to a flat earth axis system. The equations which describe the earth axis displacements are developed in References 9 and 11 and are summarized in Appendix D.

In the vehicle stability program, the altitude and free stream Mach number are considered constant; thus, the air density remains invariant. Furthermore, the entry vehicle is assumed axisymmetric and its aerodynamic force and moment characteristics are assumed specified at a point in the plane of symmetry; this point is called the balance center in Figure 3. Because the capsule is axisymmetric, body side force, yawing moment, and rolling moment about the balance center are neglected. Consequently, only body lift, drag, and pitching moment about the balance center are included in Equations (13) - (18) and these aerodynamic characteristics are transferred to the body center of gravity.

In calculating the vehicle stability time histories, the rotor airloads Equations (1) - (7) are solved initially until equilibrium is achieved in blade airloads, blade motions, and rotor torque. These rotor equilibrium hub forces and moments are then combined with the vehicle body forces and moments according to Equations (13) - (19) and integrated numerically at user-specified time increments. After each time increment, values of rotor angle of attack, rotor speed, inflow ratio, and advance ratio ($\alpha_R, \Omega, \lambda, \mu$) are compared to previous values. If the increment in these four parameters exceeds user-specified tolerances, new rotor airloads are evaluated; otherwise, the present rotor airloads are retained for the next time increment.

Further details of the computer program logic and use are presented in the user's manual (Reference 12).

CONCLUSIONS

1. The nonlinear equations of motion are derived which define blade transient responses, periodic blade airloads and kinematics, and rotor performance of fully articulated rotor systems.

2. Numerical iteration methods are developed to solve these equations of motion until equilibrium conditions are achieved.

3. A second numerical iteration method is developed to iterate on blade pitch control until the rotor autorotation criterion is satisfied.

4. The effect of capsule shock wave interaction with the rotor system is estimated by evaluating flow field characteristics ahead of and behind the shock wave line of intersection with the rotor.

5. The equations of motion for dynamic stability of the entry vehicle are modified to include rotor hub forces and moments thereby directly coupling the rotor and vehicle.

6. All of the preceding analyses are programmed in FORTRAN IV language for the Ames Research Center 7040/7094 Direct Couple System.

REFERENCES

1. Packard, C. B.: Rotochute Development for Radome Recovery Vehicle. Kaman Aircraft Report No. R-239, August 1958.

2. Barzda, J. J., et al: Investigation of Stored Energy Rotors for Recovery. USAF ASD-TDR-63-745, December 1963.

3. Levin, A. D., and Smith, R. C.: Experimental Aerodynamics of a Rotor Entry Vehicle. AIAA Preprint No. 68-950, September 1968.

4. Smith, R. C., and Levin, A. D.: The Unpowered Rotor: A Lifting Decelerator for Spacecraft Recovery. AIAA Preprint No. 68-969, September 1968.

5. Lemnios, A. Z.: The Aeroelastic Behavior of Rotary Wings in Forward Flight. The University of Connecticut, Ph.D. Thesis, 1967.

6. Gessow, A., and Myers, G. C., Jr.,: Aerodynamics of the Helicopter. The Macmillan Company, 1952.

7. Moeckel, W. E.: Approximate Method for Predicting Form and Location of Detached Shock Waves Ahead of Plane or Axially Symmetric Bodies. NACA Technical Note No. 1921, July 1949.

8. Ames Research Staff: Equations, Tables, and Charts for Compressible Flow. NACA Report 1135, 1953.

9. Etkin, B.: Dynamics of Flight. John Wiley and Sons, 1959.

10. Mersman, W. A.: Self-Starting Multistep Methods for the Numerical Integration of Ordinary Differential Equations. NASA Technical Note TN D-2936, July 1965.

11. Thelander, J. A.: Aircraft Motion Analysis. Air Force Flight Dynamics Laboratory Report FDL-TDR-64-70, March 1965.

12. Giansante, N., and Metzger, R. F.: The Dynamic Behavior of Rotor Entry Vehicle Configurations; II - Digital Computer Program Manual. Kaman Aircraft Report No. R-767-2, November 1968.

APPENDIX A

ROTOR BLADE INERTIA AND AERODYNAMIC CHARACTERISTICS

Generalized Inertias

The generalized inertias used in Equations (1) - (3) are defined by the following equations and are grouped into mass, first mass moment, and second mass moment integrals. Third and fourth order inertial terms are neglected.

$$M = \int dm \qquad I_1 = \int (r - e_2)^2 dm$$

$$I_2 = \int (r - e_2) \xi \, \$_{\theta_x} dm$$

$$S_1 = \int (r - e_2) dm \qquad I_3 = \int (r - e_2) \xi \, \mathbb{C}_{\theta_x} dm$$

$$S_2 = \int \xi \, \$_{\theta_x} dm \qquad I_4 = \int \xi^2 dm$$

$$S_3 = \int \xi \, \mathbb{C}_{\theta_x} dm \qquad I_5 = \int \xi^2 \mathbb{C}^2_{\theta_x} dm \qquad \text{(A1)}$$

Generalized Forces

The generalized forces used in Equations (1) - (3) are defined by the following equations.

$$\frac{Q_\beta}{I_1 \Omega^2} = \frac{\gamma}{2} \int_{\bar{e}_2}^{1.0} \bar{U}^2 \frac{c}{c_0} \frac{(x - \bar{e}_2)}{a} \left\{ \left[C_L + \frac{c}{R\bar{U}} \frac{dC_L}{d\alpha} \dot{\alpha} \right] \mathbb{C}_\phi + C_D \$_\phi \right\} dx \qquad \text{(A2)}$$

where $\bar{U} = \dfrac{U}{\Omega R}$

$$\frac{Q_\theta}{I_1\Omega^2} = \frac{\gamma}{2}\int_{\bar{e}_2}^{1.0}\bar{U}^2\frac{c^2}{c_0 R a}\left\{C_M + \frac{c}{R\bar{U}}\frac{dC_M}{d\alpha}\dot{\alpha} + \frac{\xi_a}{c}\right.$$

$$\left.\left[\left(C_L + \frac{c}{R\bar{U}}\frac{dC_L}{d\alpha}\dot{\alpha}\right)\mathbb{C}_a + C_D\mathbb{S}_a\right]\right\}dx \qquad \text{(A3)}$$

$$\frac{Q_\zeta}{I_1\Omega^2} = \frac{\gamma}{2}\int_{\bar{e}_1}^{1.0}\bar{U}^2\frac{c(x-\bar{e}_1)}{c_0 a}\left\{\left[C_L + \frac{c}{R\bar{U}}\frac{dC_L}{d\alpha}\dot{\alpha}\right]\mathbb{S}_\phi\right.$$

$$\left. - C_D\mathbb{C}_\phi\right\}dx \qquad \text{(A4)}$$

The directions for positive generalized forces are indicated in Figure 4. In these equations, it is assumed that the lift deficiency function C(k) = 1. The local section angle of attack and velocity components are shown in Figure 5 and are given by the following equations.

$$\alpha = \theta + \theta_x + \phi \qquad \text{(A5)}$$

$$U_P = \Omega R\left\{\lambda\mathbb{C}_\beta - (x-\bar{e}_2)\frac{d\beta}{d\psi} - \mu\mathbb{S}_\beta\mathbb{C}_{\psi+\zeta}\right\} + x\left\{q\mathbb{C}_\psi - p\mathbb{S}_\psi\right\} \qquad \text{(A6)}$$

$$U_T = \Omega R\left\{\bar{e}_1 + \left[(\bar{e}_2-\bar{e}_1) + (x-\bar{e}_2)\mathbb{C}_\beta\right]\left(1+\frac{d\zeta}{d\psi}\right) + \mu\mathbb{S}_{\psi+\zeta}\right\} \qquad \text{(A7)}$$

$$U^2 = U_T^2 + U_P^2 \qquad \text{(A8)}$$

$$\phi = \tan^{-1}\frac{U_P}{U_T} \qquad \text{(A9)}$$

APPENDIX B

CAPSULE SHOCK WAVE INTERCEPT WITH ROTOR

Figure 2 illustrates the rotor entry vehicle at an arbitrary angle of attack relative to the free stream velocity. Superposed on this vehicle are the approximate sphere and its associated detached shock wave as described in Reference 7. It is assumed that the rotor advance ratio, rotor tip speed, rotor angle of attack, and vehicle attitude are known a priori. The free stream Mach number can be evaluated from these parameters.

$$M_\infty = \frac{\mu \Omega R}{a_\infty \mathbb{C}_{a_R}} \tag{B1}$$

If $\alpha_R = \pi/2$, the free stream Mach number is expressed as

$$M_\infty = \frac{\Omega R}{a_\infty} \left(\lambda + \frac{C_T}{2\lambda} \right)$$

where C_T is the rotor thrust coefficient

$$C_T = \frac{T}{\rho \pi R^2 (\Omega R)^2}$$

and λ is the rotor inflow ratio

$$\lambda = \frac{V \sin \alpha_R - v}{\Omega R}$$

The hyperbolic shock wave defined in Reference 7 can be described in the x_o, y_c, z_o wind axis coordinate system as a function of the hyperbola semi-transverse axis (A) and the stand-off distance between the sphere and the bow wave (Δ). Figure 2 shows these dimensions and the appropriate axes; they are tabulated below versus free stream Mach number.

M	A/Rc	Δ/Rc
1.5	4.10	0.540
2.0	6.41	0.340
2.5	9.94	0.225
3.0	14.80	0.180
3.5	20.80	0.160
4.0	26.80	0.150

At intermediate Mach numbers, A and Δ can be evaluated by linear interpolation.

The equation in the wind axis system for the hyperboloid is

$$\frac{x_0^2}{A^2} - \frac{y_0^2 + z_0^2}{\left(\frac{A^2}{M_\infty^2 - 1}\right)} = 1 \qquad \text{(B2)}$$

In order to describe the line of intersection between this shock wave surface and an offset flapping rotor, Equation (B2) must be transformed into the rotor axis system. This transformation requires a standard sequence of translations and rotations as described in Reference 5. The resulting expression for the hyperboloid in rotor axis coordinates is

$$\frac{\left[x_R \mathbb{C}_{aR} + (z_R + B_{eq})\mathbb{S}_{aR} + (A + R_C + \Delta)\right]^2}{A^2} - \frac{\left[x_R \mathbb{S}_{aR} - (z_R + B_{eq})\mathbb{C}_{aR}\right]^2 + y_R^2}{\left(\frac{A^2}{M_\infty^2 - 1}\right)} = 1 \qquad \text{(B3)}$$

where B_{eq} is the distance between the rotor hub and the center of the equivalent capsule sphere.

The coordinates of a point on the blade are given by

$$\begin{aligned} x_R &= \left[e_2 + (r - e_2)\mathbb{C}_\beta\right]\mathbb{C}_\psi \\ y_R &= \left[e_2 + (r - e_2)\mathbb{C}_\beta\right]\mathbb{S}_\psi \\ z_R &= (r - e_2)\mathbb{S}_\beta \end{aligned} \qquad \text{(B4)}$$

Substitution of coordinates (B4) into Equation (B3) results in the following quadratic equation which describes the desired line of intersection.

$$\begin{aligned} &\left\{C_1^2 - \left[C_2^2 + \mathbb{C}_\beta^2 \mathbb{S}_\psi^2\right](M_\infty^2 - 1)\right\}(r - e_2)^2 \\ &+ 2\left\{C_1 C_3 - \left[C_2 C_4 + e_2 \mathbb{C}_\beta \mathbb{S}_\psi^2\right](M_\infty^2 - 1)\right\}(r - e_2) \\ &+ \left\{C_3^2 - \left[C_4^2 + e_2^2 \mathbb{S}_\psi^2\right](M_\infty^2 - 1) - A^2\right\} = 0 \end{aligned} \qquad \text{(B5)}$$

where

$$C_1 = \$_{a_R}\$_\beta + \mathbb{C}_{a_R}\mathbb{C}_\beta\mathbb{C}_\psi$$

$$C_2 = \mathbb{C}_{a_R}\$_\beta - \$_{a_R}\mathbb{C}_\beta\mathbb{C}_\psi$$

$$C_3 = B_{eq}\$_{a_R} + e_2\mathbb{C}_{a_R}\mathbb{C}_\psi + A + R_C + \Delta$$

$$C_4 = B_{eq}\mathbb{C}_{a_R} - e_2\$_{a_R}\mathbb{C}_\psi$$

The periodic variation of blade flapping angle with rotor azimuth position is known from the numerical solution of Equations (1) - (3). Thus, the coefficients C_1, C_2, C_3, C_4 and the coefficients of Equation (B5) can be numerically evaluated at any azimuth position, ψ . The resulting quadratic equation at each azimuth can be solved for $(r-e_2)$.

APPENDIX C

VEHICLE STABILITY EQUATIONS

Equations (13) - (15) can be solved directly for the linear accelerations in the body axis system as shown below.

$$\dot{u}_B = \frac{F_{x_B}}{M_B} + g\,\mathbb{S}_{\theta_E} + \frac{F_{x_R}}{M_B} + v_B r_B - w_B q_B \tag{C1}$$

$$\dot{v}_B = \frac{F_{y_B}}{M_B} - g\,\mathbb{C}_{\theta_E}\mathbb{S}_{\phi_E} + \frac{F_{y_R}}{M_B} + w_B p_B - u_B r_B \tag{C2}$$

$$\dot{w}_B = \frac{F_{z_B}}{M_B} - g\,\mathbb{C}_{\theta_E}\mathbb{C}_{\phi_E} + \frac{F_{z_R}}{M_B} + u_B q_B - v_B p_B \tag{C3}$$

Equation (17) can also be solved directly for the body pitch acceleration.

$$\dot{q}_B = \frac{M_{y_B} + M_{y_R} + (B_R - B_C)F_{x_R} + A_C(F_{z_R} + F_{z_B}) + (B_M - B_C)F_{x_B}}{I_{yy}} + (r_B^2 - p_B^2)\frac{I_{xz}}{I_{yy}} + r_B p_B\left(\frac{I_{zz} - I_{xx}}{I_{yy}}\right) \tag{C4}$$

Equation (18) can be written to express yaw acceleration in terms of roll acceleration.

$$\dot{r}_B = -\frac{A_C(F_{y_R} + F_{y_B})}{I_{zz}} + (\dot{p}_B - q_B r_B)\frac{I_{xz}}{I_{zz}} + \left(\frac{I_{xx} - I_{yy}}{I_{zz}}\right)p_B q_B \tag{C5}$$

Substitution of this relation into Equation (16) yields the following expression for roll acceleration.

$$\dot{p}_B = \left\{ M_{x_g} + M_{x_R} - (B_R - B_C) F_{y_R} - (B_M - B_C) F_{y_B} \right\} \frac{I_{zz}}{I_{xx} I_{zz} - I_{xz}^2}$$

$$- \left\{ A_C (F_{y_B} + F_{y_R}) \right\} \frac{I_{xz}}{I_{xx} I_{zz} - I_{xz}^2}$$

$$+ \left\{ \frac{(I_{yy} - I_{zz}) I_{zz} - I_{xz}^2}{I_{xx} I_{zz} - I_{xz}^2} \right\} q_B r_B + \frac{I_{xz} (I_{xx} - I_{yy} + I_{zz})}{I_{xx} I_{zz} - I_{xz}^2} \Bigg\} p_B q_B \qquad \text{(C6)}$$

Finally, the rotor deceleration is simply

$$\dot{\Omega} = \dot{r}_B - \frac{Q}{I_R} \qquad \text{(C7)}$$

where Q is the torque due to airloads as defined in Equation (4).

Because of the axisymmetric characteristics of the capsule mentioned in a previous section, the body forces and moments given in Equations (C1) - (C7) are related to the reference center lift, drag, and pitching moment by

$$F_{x_B} = (D_B \mathbb{C}_{\alpha_B} - L_B \$_{\alpha_R}) \mathbb{C}_\eta$$

$$F_{y_B} = (D_B \mathbb{C}_{\alpha_B} - L_B \$_{\alpha_R}) \$_\eta$$

$$F_{z_B} = (D_B \$_{\alpha_R} + L_B \mathbb{C}_{\alpha_R})$$

$$M_{x_B} = - \hat{M}_{y_B} \$_\eta$$

$$M_{y_B} = \hat{M}_{y_B} \mathbb{C}_\eta \qquad \text{(C9)}$$

$$M_{z_B} = - A_C F_{y_B}$$

where $\hat{M}_{y_B}$ is defined in Equation (C13).

The rotor hub forces and moments in Equations (C1) - (C7) are

$$F_{x_R} = H\mathbb{C}_\eta - Y\mathbb{S}_\eta$$

$$F_{y_R} = Y\mathbb{C}_\eta + H\mathbb{S}_\eta$$

$$F_{z_R} = T$$

$$M_{x_R} = -(B_R - B_C)\{Y\mathbb{C}_\eta + H\mathbb{S}_\eta\} + \hat{M}_{x_R}\mathbb{C}_\eta - \hat{M}_{y_R}\mathbb{S}_\eta$$

$$M_{y_R} = (B_R - B_C)\{H\mathbb{C}_\eta - Y\mathbb{S}_\eta\} + \hat{M}_{x_R}\mathbb{S}_\eta + \hat{M}_{y_R}\mathbb{C}_\eta \qquad \text{(C10)}$$

where $\hat{M}_{x_R}$ and $\hat{M}_{y_R}$ are defined by Equations (C16).

In Equations (C9) and (C10), the angle η, between the relative wind and the X-axis is defined as follows:

$$\eta = \tan^{-1}\frac{v_B}{u_B} \qquad \text{(C11)}$$

The set of equations given by (C1) - (C11) can be solved numerically after initial conditions are specified and backward differences are calculated as described in Reference 10. After the pitch and roll rates of the body are calculated from the preceding equations, they are transformed into pitch and roll rates in the rotor axes according to the following equations.

$$q = q_B\mathbb{C}_\eta - p_B\mathbb{S}_\eta$$

$$p = q_B\mathbb{S}_\eta + p_B\mathbb{C}_\eta \qquad \text{(C12)}$$

The pitch and roll rates from Equation (C12) are then transmitted back to the blade equations of motion and used to evaluate new equilibrium airloads and blade kinematics.

The capsule body lift (L_B) and drag (D_B) forces are calculated using the plan area of the capsule body as a reference. The body pitching moment (M_{Y_B}) is also a function of the aforementioned reference area and capsule body diameter.

$$L_B = \frac{\pi}{2} \rho V_\infty^2 R_C^2 C_{L_{RC}}$$

$$D_B = \frac{\pi}{2} \rho V_\infty^2 R_C^2 C_{D_{RC}}$$

$$\hat{M}_{y_B} = \pi \rho V_\infty^2 R_C^3 C_{m_{RC}} \qquad \text{(C13)}$$

where the subscript RC refers to the body reference center.

The rotor hub moments due to the vertical shear forces acting at the flapping hinge are calculated in the rotor axis system and resolved into the body coordinate system. These vertical shears include forces resulting from aerodynamics, flapping accelerations and pitch and roll rates.

The vertical shear acting at the blade flapping hinge at any azimuth position can be expressed as:

$$\frac{dFv}{d\psi} = \frac{dT}{d\psi} - S_1 \Omega \left[\Omega \left(\frac{d^2\beta}{d\psi^2} \right) + 2(q\$_\psi + p\mathbb{C}_\psi) \right] \mathbb{C}_\beta \qquad \text{(C14)}$$

The contribution to the moments about the blade flapping and feathering axes due to spring and damper effects at any azimuth position can be expressed as

$$\frac{dM_\beta}{d_\psi} = -C_\beta \Omega \frac{d\beta}{d\psi} - K_\beta (\beta - \beta_0) - K_{\theta_{IN}} K_{\theta\beta} (K_{\theta\beta}\beta + \theta_{IN} - \theta + K_{\theta\zeta}\zeta)$$

$$\frac{dM_\theta}{d\psi} = -C_\theta \Omega \frac{d\theta}{d\psi} - K_\theta (\theta - \theta_0) - K_{\theta_{IN}} (\theta - K_{\theta\beta}\beta - K_{\theta\zeta}\zeta - \theta_{IN}) \qquad \text{(C15)}$$

The moments due to this force, and these moments resolved into the body coordinate system are:

$$\frac{dMx}{d\psi} = +\frac{dFv}{d\psi}\left\{(e_2 - e_1)\,\mathbb{S}_{\psi-\zeta} + e_1\,\mathbb{S}_{\psi}\right\} + \frac{dM\beta}{d\psi}\,\mathbb{S}_{\psi-\zeta} + \frac{dM\theta}{d\psi}\,\mathbb{C}_{\psi-\zeta}$$

$$\frac{dMy}{d\psi} = -\frac{dFv}{d\psi}\left\{(e_2 - e_1)\,\mathbb{C}_{\psi-\zeta} + e_1\,\mathbb{C}_{\psi}\right\} - \frac{dM\beta}{d\psi}\,\mathbb{C}_{\psi-\zeta} + \frac{dM\theta}{d\psi}\,\mathbb{S}_{\psi-\zeta} \qquad \text{(C16)}$$

Integrating these expressions around the azimuth yields the rotor average moments about the body X and Y axes.

$$\hat{M}_{x_R} = \frac{b}{2\pi}\int_0^{2\pi} \frac{dMx}{d\psi}\,d\psi$$

$$\hat{M}_{y_R} = \frac{b}{2\pi}\int_0^{2\pi} \frac{dMy}{d\psi}\,d\psi \qquad \text{(C17)}$$

APPENDIX D

EARTH AXIS DISPLACEMENTS

The linear and rotational velocities and displacements of the rotor entry vehicle in flat earth axis coordinates can be calculated from the results of the coupled rotor-body equations of motion in Appendix C. The relationships between the body velocities and earth axis velocities are given below.

$$\dot{\Theta}_E = q_B \mathbb{C}_{\Phi_E} - r_B \mathbb{S}_{\Phi_E} \tag{D1}$$

$$\dot{\Phi}_E = p_B + (q_B \mathbb{S}_{\Phi_E} + r_B \mathbb{C}_{\Phi_E}) \mathbb{S}_{\theta_E} / \mathbb{C}_{\theta_E} \tag{D2}$$

$$\dot{\Psi}_E = (q_B \mathbb{S}_{\Phi_E} + r_B \mathbb{C}_{\Phi_E}) / \mathbb{C}_{\theta_E} \tag{D3}$$

$$\dot{X}_E = \left\{ u_B \mathbb{C}_{\theta_E} + (v_B \mathbb{S}_{\Phi_E} + w_B \mathbb{C}_{\Phi_E}) \mathbb{S}_{\theta_E} \right\} \mathbb{C}_{\Psi_E} - \left\{ v_B \mathbb{C}_{\Phi_E} - w_B \mathbb{S}_{\Phi_E} \right\} \mathbb{S}_{\Psi_E} \tag{D4}$$

$$\dot{Y}_E = \left\{ u_B \mathbb{C}_{\theta_E} + (v_B \mathbb{S}_{\Phi_E} + w_B \mathbb{C}_{\Phi_E}) \mathbb{S}_{\theta_E} \right\} \mathbb{S}_{\Psi_E} + \left\{ v_B \mathbb{C}_{\Phi_E} - w_B \mathbb{S}_{\Phi_E} \right\} \mathbb{C}_{\Psi_E} \tag{D5}$$

$$\dot{Z}_E = -u_B \mathbb{S}_{\theta_E} + (v_B \mathbb{S}_{\Phi_E} + w_B \mathbb{C}_{\Phi_E}) \mathbb{C}_{\theta_E} \tag{D6}$$

Coordinates in the earth axes are calculated by integrating Equations (D1) - (D6).

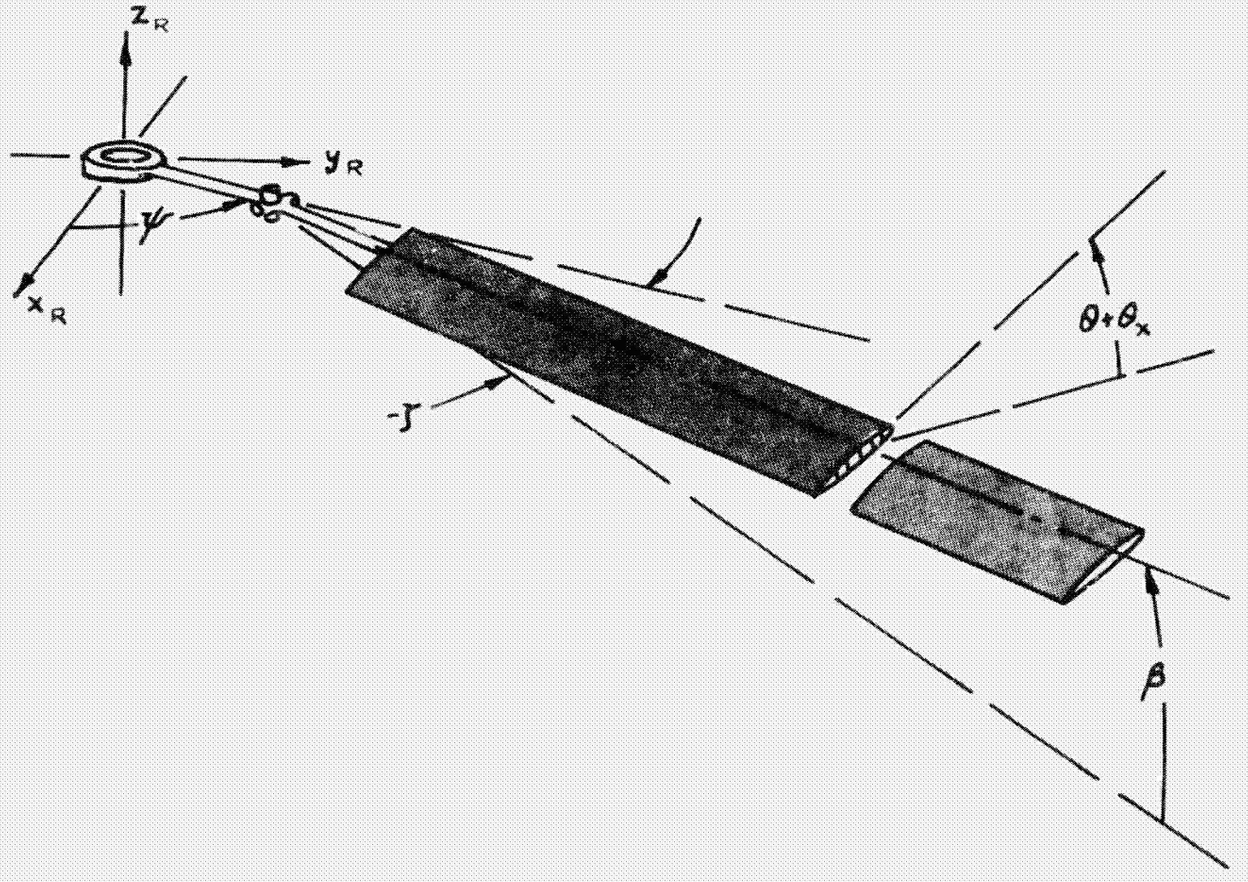

Figure 1. Geometry of Deflected Rotor Blade

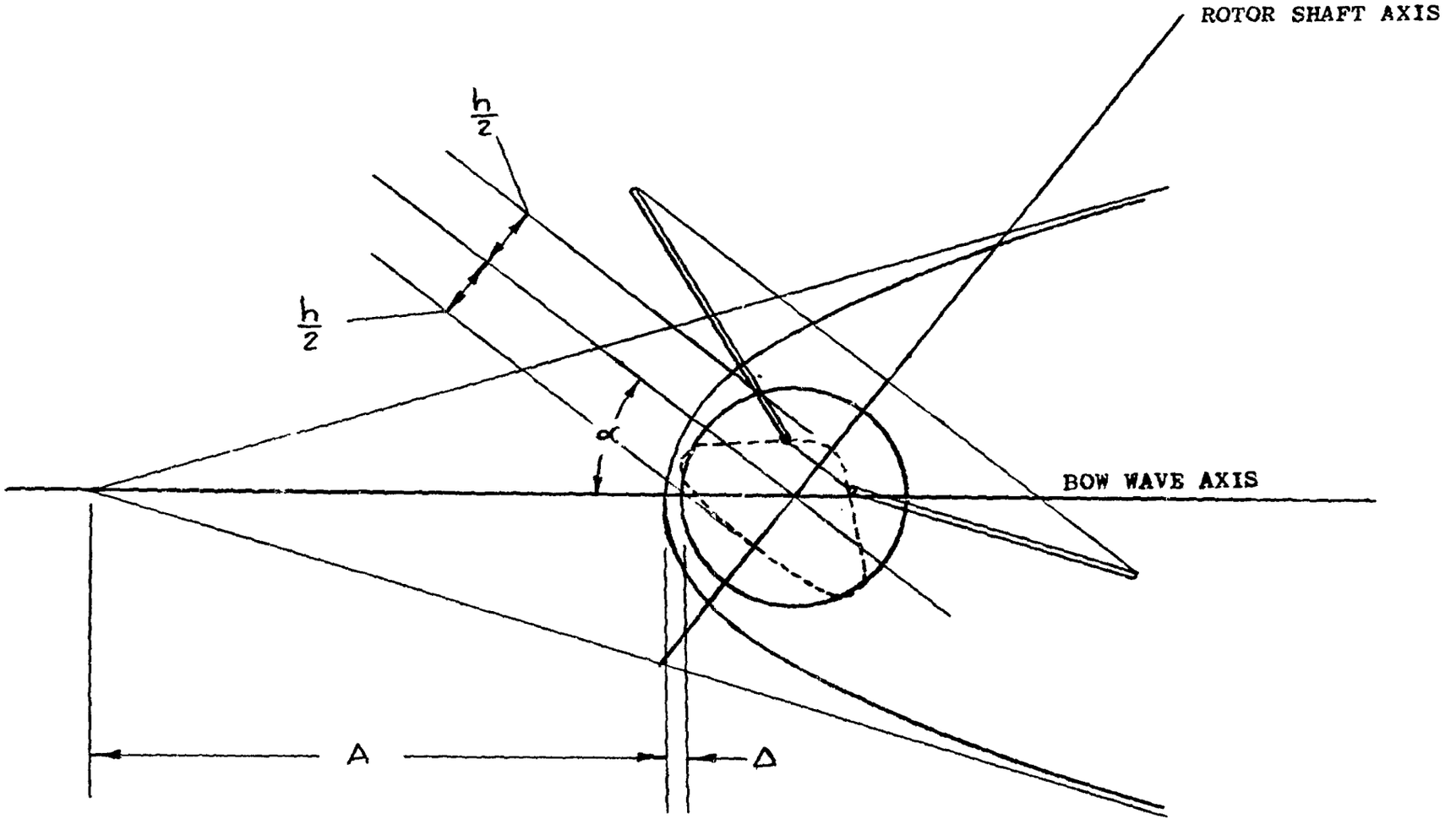

Figure 2. Configuration For Approximating Bow Wave Shape

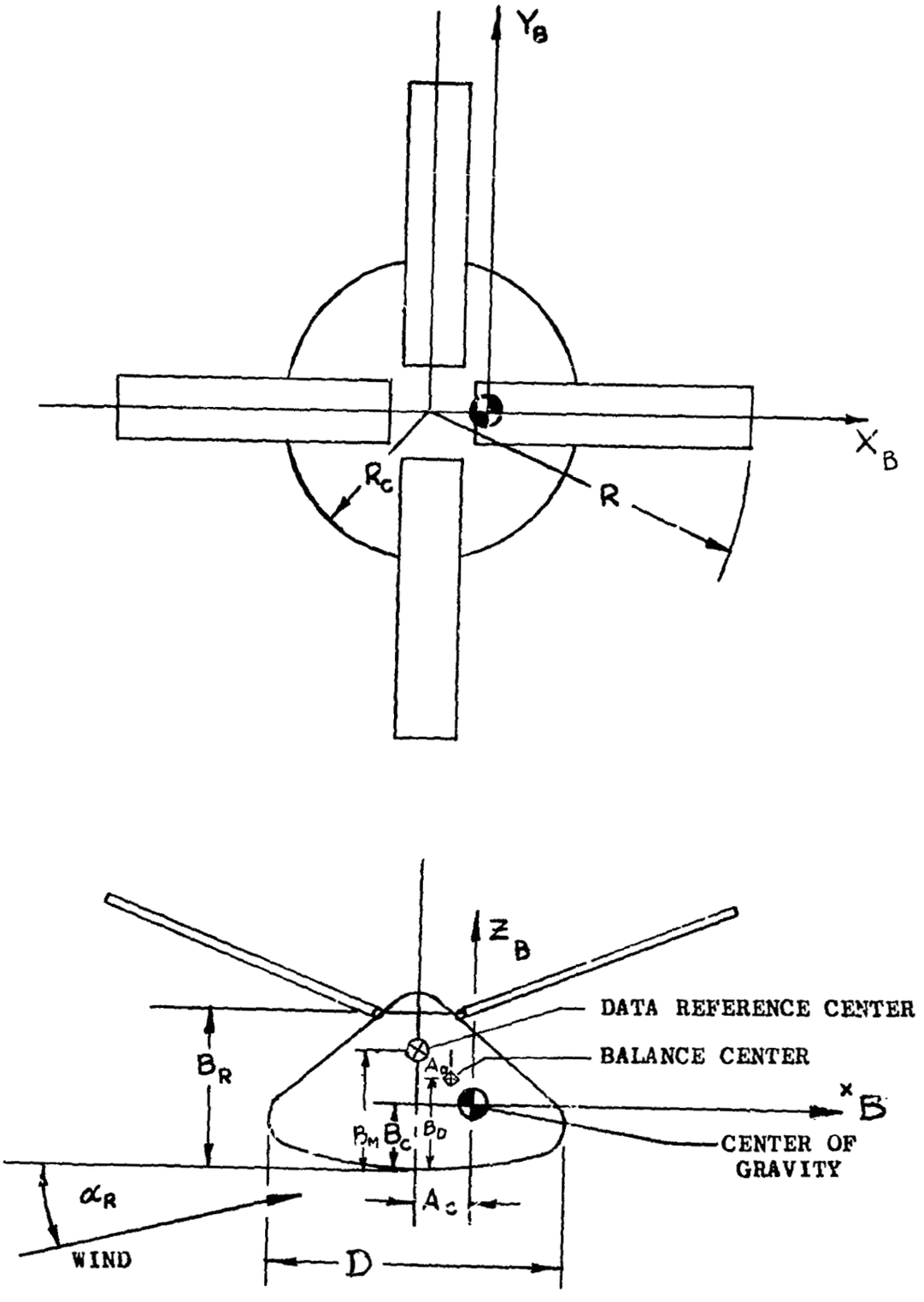

Figure 3. Vehicle Configuration For Dynamics Study

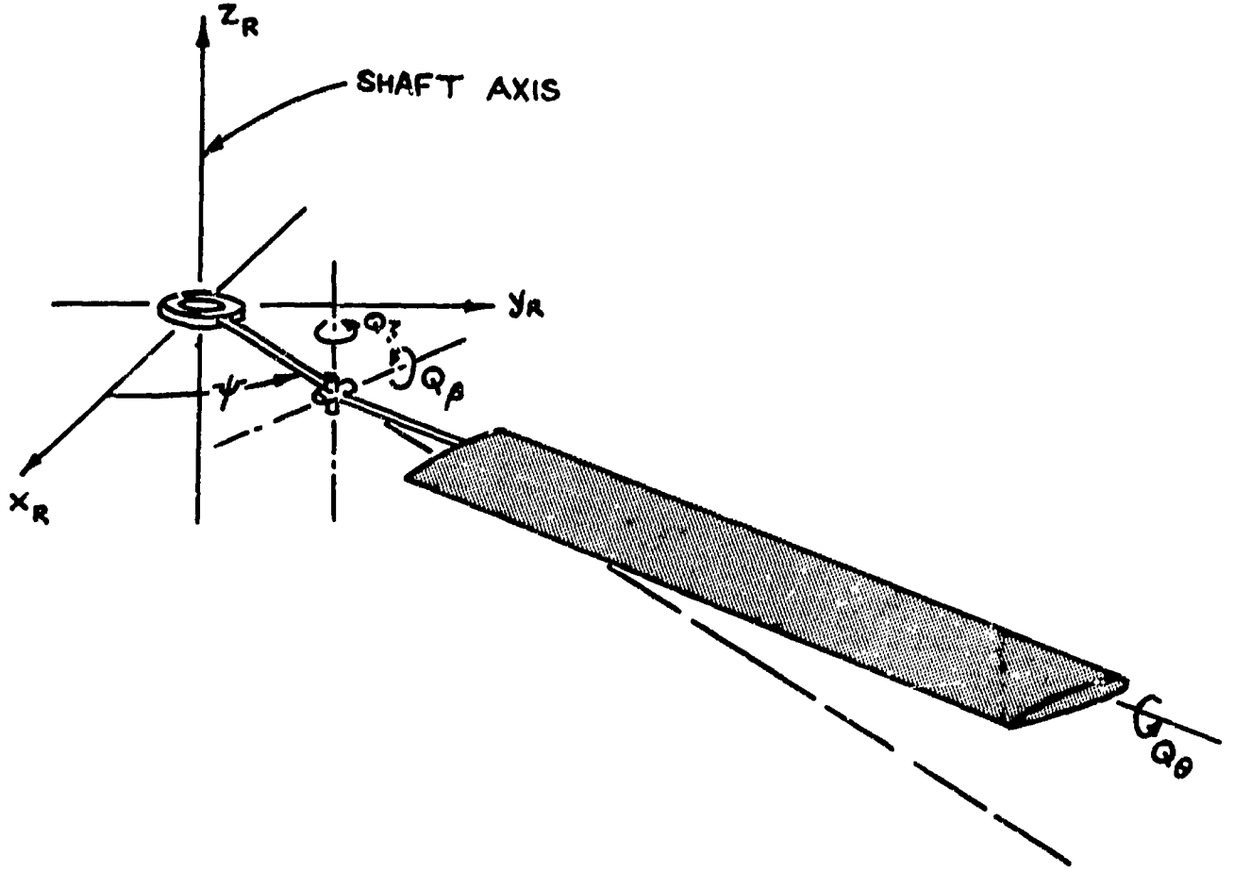

Figure 4. Generalized Forces Of The Rotor System

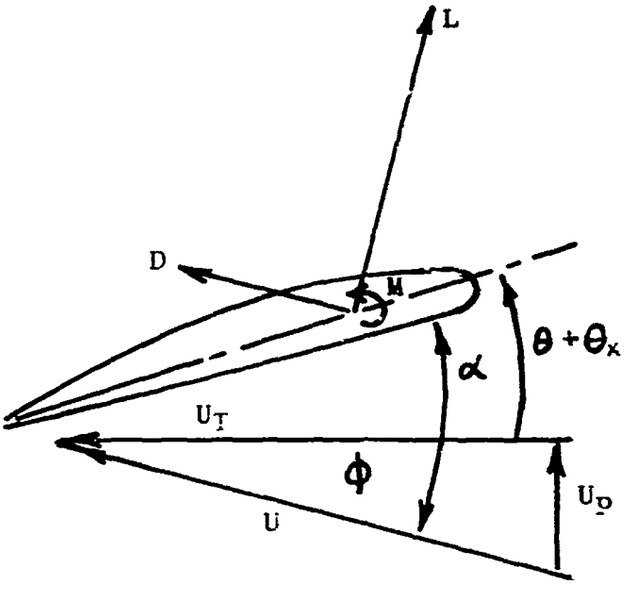

Figure 5. Airfoil Section Indicating Aerodynamic Force And Velocity Vectors

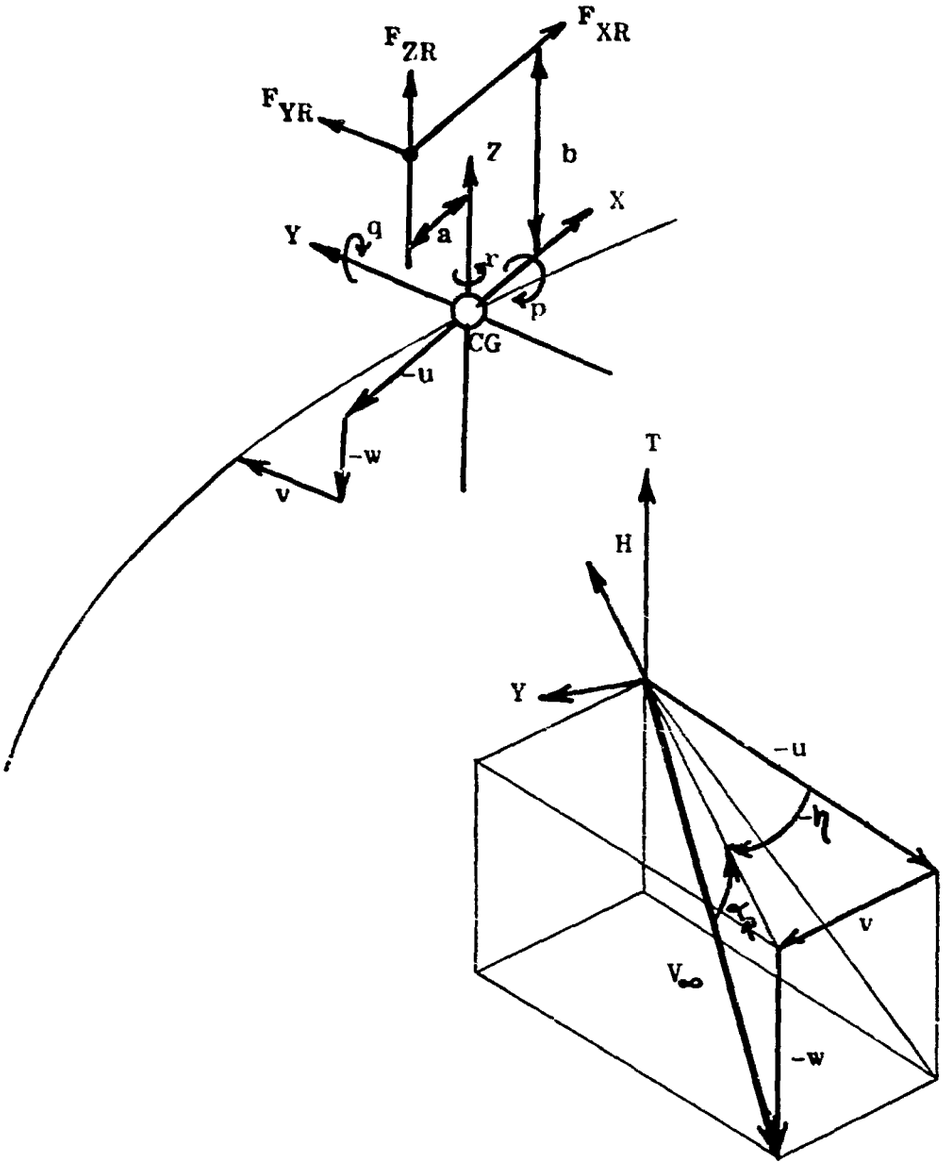

Figure 6. Rotor And Vehicle Coordinate Systems

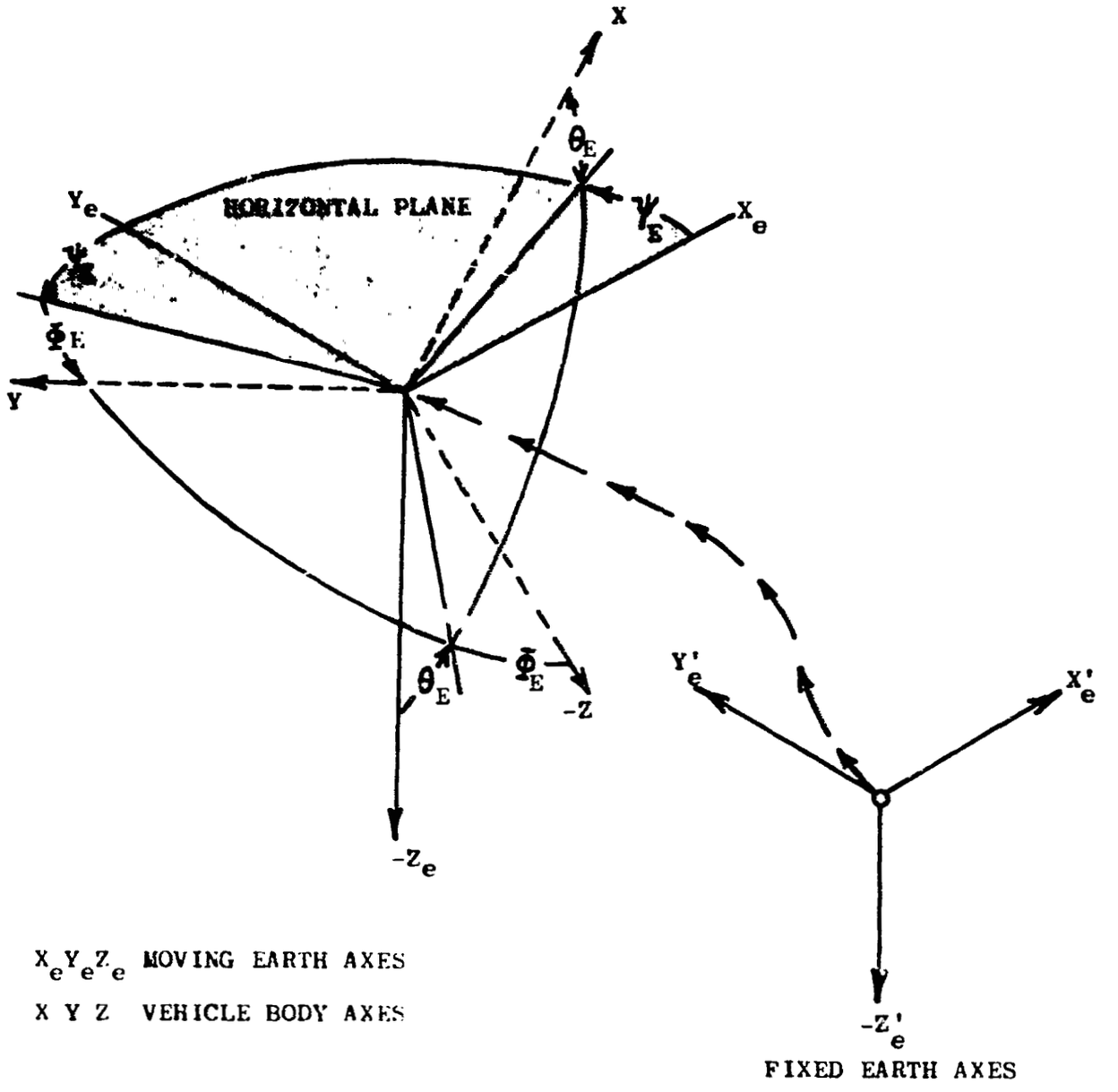

Figure 7. Rotation From Earth To Body Axes-
Yaw-Pitch-Roll Sequence